Scientific Research Publishing

Open Journal of Microphysics, 2023, 13, 36-51
https://www.scirp.org/journal/ojm
ISSN Online: 2162-2469
ISSN Print: 2162-2450

Density Functional Study of Mechanical, Electronic and Pressure Induced Phase Transition Properties of $CaFe_2As_2$

Mochama Victor Samuel[1], Calford Odhiambo Otieno[1], Phillip Nyawere[2]

[1]Department of Physics, Kisii University, Kisii, Kenya
[2]Department of Physical and Biological Sciences, Kabarak University, Nakuru, Kenya
Email: mochamavic@gmail.com

How to cite this paper: Samuel, M.V., Otieno, C.O. and Nyawere, P. (2023) Density Functional Study of Mechanical, Electronic and Pressure Induced Phase Transition Properties of $CaFe_2As_2$. *Open Journal of Microphysics*, **13**, 36-51.
https://doi.org/10.4236/ojm.2023.133004

Received: May 28, 2023
Accepted: August 4, 2023
Published: August 7, 2023

Abstract

We report results on the *ab initio* study of the mechanical and electronic properties of the iron Pnictide compound $CaFe_2As_2$ and its phase transition under pressure using Quantum Espresso code. We do analysis of the strength of bonds in individual points of this material and proper Cauchy pressure calculation which will give more insight on the elastic responses. Ground state energy was done in the framework of density functional theory (DFT) based on plane wave self-consistent field (PWscf) and ultrasoft pseudo potential (USPP) method as treated in the Perdew-Burke Ernzerhof (PBE) generalized gradient approximation and local density approximations. Elastic constants were computed using thermo_pw and the values were used to calculate mechanical properties and pressure phase changes. From the non-zero positive elastic constants, the Iron Pnictide compound is found to be mechanically stable and its Poisson's ratio indicates that it is brittle and isotropic. Pressure induced phase transition is here found to happen at an applied external pressure of 0.2 GPa causing the tetragonal phase to change to an orthorhombic phase which agrees well with previous reports.

Keywords

Phase Transition, Elastic Constants, Modulus

1. Introduction

The exposure of iron Pnictide materials superconducting at high temperatures has renewed research on their superconductivity mechanisms [1]. The superconducting iron Pnictide class of 122 compounds, are structurally simple as compared to the 111 family of Pnictides [2]. 122 class of iron pnictides has atomic

arrangement of AFe_2As_2 which is stable with divalent (A = Ba, Ca, Sr, and Eu) atoms. They crystalize at room temperature into $ThCr_2Si_2$ type tetragonal structure [3] with space group of 14/mmm [4]. $CaFe_2As_2$ as one of the 122 classes, when subjected to either conditions of pressure or temperature transits from the tetragonal stable phase to orthorhombic [5]. As our motivation, Iron Pnictide compounds have been identified to possess superconducting properties when they are either doped or subjected to the external pressure to phase transition point [6]. Electron or hole doping suppresses magnetic and structural instabilities inducing superconductivity. Application of pressure on the parent compounds suppresses magnetic order [6] and enhances superconductivity in $CaFe_2As_2$ [6] [7].

Electrons in 3d orbitals in $CaFe_2As_2$ enables electrons in low-lying electronic state with many hole and electron bands pair at low temperatures, which is one of the conditions that leads to superconductivity [8]. At the superconductivity state, $CaFe_2As_2$ is very sensitive to applied pressure and this causes it to have several phases at low temperatures. In the collapsed tetragonal shape, the electron correlation and superconductivity disappear [9] and $CaFe_2As_2$ transits to orthorhombic phase at room temperature [10]. If pressure is applied by a non-hydrostatic medium, $CaFe_2As_2$ becomes a superconductor, but small uniaxial pressure parts overturns its superconductivity [11].

$CaFe_2As_2$ on cooling through 170 K, undergoes first-order magnetic phase transition [12]. Superconductivity appears above 40 K when the single crystal of the compound is electron doped [13]. This compound contains oxide blocks on the *c*-axis and two-dimensional iron (Fe) and arsenic (As) tetrahedron layers which act as charge reservoirs and denote the structural phase transition. The presence of iron in this compound contributes to its magnetic properties which when tuned can turn on and off its superconducting behavior [14].

Na-substitution in between Ca and Fe with composition $Ca_5Na_5Fe_2As_2$ induce superconductivity at 20 K. Upon application of pressure, it lacks any sign of superconductivity but has a reduction of its unit cell volume [15]. Reduction of the unit cell volume and hole doping are very essential for superconductivity.

The objectives of this paper first are to present an elaborate calculation on density functional investigations on the electronic and mechanical properties of $CaFe_2As_2$. Secondly to study pressure induced phase transition of $CaFe_2As_2$. The rest of this paper is organized such that Section 2 is the computational methodology, Section 3 presents results, and the conclusion is in Section 4.

2. Computational Method

The first principle calculation study of $CaFe_2As_2$ under induced pressure was undertaken in the framework of density functional theory (DFT) based on plane wave self-consistent field (PWscf) and ultrasoft pseudopotential (USPP) method as treated in the Perdew-Burke Ernzerhof (PBE) [16] generalized gradient approximation and local density approximation. The computational calculations were performed using Quantum Espresso simulation package and the optimized

cell dimensions were fitted using Murnaghan fitting methodology of second order given by Equation (1). The equation gives the relationship which exists between the volume of a body and pressure upon which it is subjected. This shows that when bodies are compressed more, it becomes more difficult to compress them beyond some limit. The Murnaghan equation models experimental data with satisfactory accuracy.

$$P = 1.5B_o\left[\frac{v_O}{v}^{\frac{7}{3}} - \left(\frac{v_o}{v}\right)^{\frac{5}{3}}\right]\left[1 + 0.75\left(B_o' - 4\right)\left(\left\{\frac{v_o}{v}\right\}^{\frac{2}{3}} - 1\right)\right] \quad (1)$$

The *k*-points, and the kinetic energy cut-off values were properly checked through graphing and accurate values were obtained for the convergence of the ground state energy at minimum convergence threshold in the calculation using the proper basis sets [17]. Minimum point of convergence is essential in finding a proper initial setting in making decision on reliability and accuracy of simulation. Self-Consistency Field in Density Functional Theory determines ground state electron density through energy change which brings a slight change in electron density. Convergence is achieved when the energy reaches the global minimum. Convergence is achieved by a set threshold whereby a smaller threshold produces more accurate results. The minimization is given by the relation in Equation (2):

$$E\left(V\right) = E_o + \frac{9V_oB_o}{16}\left\{\left[\left(\frac{V_o}{V}\right)^{\frac{2}{3}} - 1\right]^3 B_o' + \left[\left(\frac{V_o}{V}\right)^{\frac{2}{3}} - 1\right]^2\left[6 - 4\left(\frac{V_o}{V}\right)^{\frac{2}{3}}\right]\right\} \quad (2)$$

The valence configuration used for $CaFe_2As_2$ was $3s^23p^64s^2$ for Ca, $3s^24s^23p^6$ for Fe and $4s^24p^3$ for As. The convergence threshold was estimated at 10^{-8} eV which is sound for accuracy. The Brillouin sampling was based on the Monkhost scheme [18] where K-point mesh of the irreducible high symmetry points in the Brillouin zone used was 6 × 6 × 4. For the elastic constant calculation, the 'quasi-static' approximation was used, where the elastic constants were computed at absolute temperature and saved as elastic constants.

Mechanical properties play significant role in the crystal structure studies. Empirically, mechanical properties of materials are determined by elastic properties which include the shear modulus (G), bulk modulus (B), Young modulus (E), and Poisson's ratio (*n*).

Specifically, elastic properties are achieved by the elastic constants (C_{ij}), which are identified as the stress tensor versus small strain. Additionally, the mechanical stability of materials is calculated by elastic constants. For cubic crystal structure, there exist three independent elastic constants; C_{11}, C_{12}, and C_{44}, which determine the mechanical stability given by Born-Huang's stability criteria [19] [20] in Equation (3):

$$\begin{aligned} &C_{ii} > 0\left(i = 1,3,4,6\right) \\ &C_{11} + C_{33} - 2C_{13} > 0 \\ &2\left(C_{11} + C_{12}\right) + C_{33} + 4C_{13} > 0 \end{aligned} \quad (3)$$

$$C_{11} - C_{12} > 0$$

Taking into account the structural symmetry, the shear and bulk moduli are evaluated in compliance with Voigt-Reuss-Hill (VRH) approximation. Additionally, the Young's modulus is identified as the ratio of linear strain versus linear stress, which gives the degree of elastic stiffness. Poisson's ratio indicates the advances of the covalent bond. A high ratio proves the presence of ionic and metallic bonds. Values of C_{ij} can be used in the evaluation of Poisson's ratio and elastic moduli of $CaFe_2As_2$. As per Voigt approximation, the bulk and shear moduli isotropy can be acquired by doing linear combination of elastic constants [20]. With a different format, Reuss obtained estimates for bulk and shear moduli isotropy by employing the use of single crystal elastic constants. Hill confirmed that Voigt and Reuss estimates were lower and upper polycrystalline elastic moduli limits respectively, hence the averages became realistic as shown in Equation (4).

$$B = \frac{B_V + B_R}{2}$$

$$G = \frac{G_V + G_R}{2} \tag{4}$$

Elastic anisotropy calculation is an important aspect as it gives important information on the likelihood of the introduction of micro cracks in the compounds in trying to improve their durability [21]. We calculate the elastic anisotropy factor *(A)* by making use of the following Equations (5-7). The shear anisotropic factor for the {1 0 0} shear planes between the <011> and <010> directions is:

$$A_1 = \frac{4C_{44}}{C_{11} + C_{55} - 2C_{13}} \tag{5}$$

For the {0 1 0} shear planes between <101> and <001> directions it is:

$$A_2 = \frac{4C_{55}}{C_{22} + C_{33} - 2C_{23}} \tag{6}$$

For the {0 0 1} shear planes between <110> and <010> directions it is

$$A_3 = \frac{4C_{66}}{C_{11} + C_{22} - 2C_{12}} \tag{7}$$

But since our crystal does not have C_{22} and C_{55} our calculations of shear anisotropic factors is only for A_1 which is 1.0914 showing that our compound is isotropic.

Another important mechanical property of materials is the Vickerhardness H_v. The Vicker hardness test determines the hardness of a material. It also helps in testing hardness in thin layers in trying to overcome the problem of cracking in brittle materials. It can be predicted by Equation (8) [22]:

$$H_v = 0.92\left(B/G\right)^{1.3137} G^{0.708} \tag{8}$$

Materials with Vicker's hardness beyond 40 GPa are considered to be super-

hard materials. The Vicker's hardness to our compound is 18.1193 GPa an indication that the compound is not hard enough to resist being dented.

Debye temperature is another basic physical property which distinguishes between low and high temperature regions for a given material. We calculated the Debye temperature for this compound by the use of the following formula [23]:

$$\theta_D = \frac{h}{K_B}\left[6\pi^2 V^{\frac{1}{2}} n\right] f(\sigma)\sqrt{\frac{B_S}{M}}$$

$$f(\sigma) = \left\{3\left[2\left(2/3\frac{1+\sigma}{1-2\sigma}\right)^{3/2} + \left(1/3\frac{1+\sigma}{1-\sigma}\right)^{3/2}\right]^{-1}\right\}^{\frac{1}{3}} \quad (9)$$

where V is the unit cell volume, n number of atoms in a unit cell, B_S bulky modulus, M molar mass, σ poisson ratio. The calculated Debye temperature is 3.8707 K hence we expect frozen high frequency modes [24].

Pressure, which is the main basis for phase transition, was calculated for a good range of volume by the relationship of Equation (10):

$$H(P) = U(V[P]) + PV \quad (10)$$

Structural transition is associated with the atomic packing and orientation in the crystal, which brings about the change of the related properties of the compound. This change is due to different conditions, for instance, temperature and pressure. Given that our calculations are done at ground state temperature, only the pressure is varied in these calculations.

3. Results and Discussion

Superconductivity of this material which is the main focus of this study appears at structural phase transition point brought about by the application of external pressure. This brings the need to understand structural properties of $CaFe_2As_2$.

3.1. Structural and Mechanical Properties

Optimization of the cut-off energy convergence was achieved at *45 Ry*. **Figure 1** shows the optimized structure of $CaFe_2As_2$.

The optimized cell parameter a = 3.97 Å and c = 12.84 Å, which agrees well with experimental and other theoretical work as shown in **Table 1** below.

Optimization of parameters such as lattice constants and cut-off energy was done to obtain a relaxed structure free from stress [25].

Table 2 gives results of the elastic constants of $CaFe_2As_2$ as calculated in this work and reported for the first time.

Elastic constants C_{11} and C_{33} portray the level of deformation resistance along the *a*-axis and *c-axis,* respectively. Evaluated elastic constant C_{11} for $CaFe_2As_2$ is greater than that of elastic constant C_{33} by around 39.9%, a clear indication that this compound contains strong deformation resistance along the *a*-axis compared to *c*-axis.

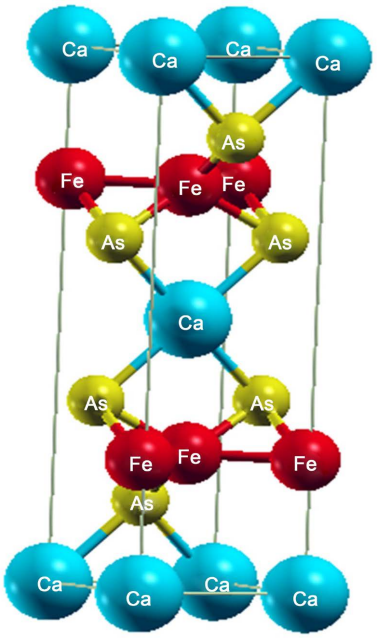

Figure 1. Crystal structure of $CaFe_2As_2$ as visualized from quantum espresso Xcrysden package, $a = b \neq c$.

Table 1. Comparison of experimental and theoretical cell dimensions.

Parameter	Our work	Experimental	Theoretical	Reference
$a_0 = b_0$ (Å)	3.97	3.887	3.829	[26] [27]
c_0 (Å)	12.84	11.758	11.862	[26] [27]

Table 2. Elastic constants of tetragonal $CaFe_2As_2$.

C_{ij}	GPa
C_{11}	88.86
C_{12}	22.58
C_{13}	28.63
C_{33}	63.51
C_{44}	25.93
C_{66}	25.93

On the other side, the elastic constant C_{44} describes the extent of shear distortion in the [1 0 0] plane, while the elastic constant C_{66}indicates the shear resistance in the [1 1 0] direction [28]. This compound's elastic constants satisfy the requirement for mechanical stability conditions given by Equation (5). Elastic constants C_{44} and C_{66} of $CaFe_2As_2$ obtained are 25.95 GPa and 31.73 GPa which are far less than other iron pnictides, a clear indication that $CaFe_2As_2$ has a lower deformation resistance compared to other iron pnictides. Deformation resistance is extensively accepted as a crucial engineering property of asphalt used for

surfacing and construction of roads [29]. A higher deformation resistance indicates reduced potential for asphalt shearing, rutting and shoving mainly under heavy and slow moving loads making $CaFe_2As_2$ non effective.

The Young's modulus E and Poisson's ratio n and their relationships with bulk modulus and shear modulus are as tabulated in **Table 3** below [30].

Shear modulus indicates strength of the material unlike the bulk modulus. We have determined that $G > B$, hence $CaFe_2As_2$ mechanical failure should be corrected by application of the shear component. Bulk modulus B reveals the extent to which a material is compressible in relation to another. The higher the value of B, the incompressible the material is [31]. $BaFe_2As_2$ is more incompressible than $CaFe_2As_2$ with a value of 71 GPa. The Poisson's ratio [32] determines ductility or brittleness of the material. The higher the ratio, the more ductile the material is, whereas a low value indicates less brittleness. For $\frac{B}{G} > 1.75$ indicates ductility otherwise the material is brittle. $\frac{B}{G}$ shows that the hardness is related inversely, meaning that the smaller the ratio, the harder the material. $CaFe_2As_2$ is hard and brittle with $\frac{B}{G} = 0.655935$. Poisson's ratio (n) also helps us to assess the mechanical properties of crystalline solids. Its low value indicates stability against shear [33]. Poisson's ratio at the same time reveals the nature of interatomic forces where a range of 0.25 and 0.50 indicates central force interaction and outside this range for non-central force interactions. Moreover according to Poisson's ratio, materials whose ratio is less than 0.26 undergo brittle failure, but above this ratio they undergo ductile failure. Poisson's ratio of $CaFe_2As_2$ shows that it is brittle [34]. Resistance to compressive or expansive forces is measured by Young's modulus. From **Table 3**, the value of E is small, even smaller than that of $BaFe_2As_2$ of 101.6 GPa, indicating that $CaFe_2As_2$ definitely cannot withstand large tensile stress [35].

Cauchy pressure [36] is the difference between C_{12} and C_{44} elastic constants. This parameter reveals more about the elastic response and large density of solids. Cauchy pressure will indicate ductility or brittleness failure of crystalline solids. A positive and negative Cauchy pressure indicates ductility and brittleness, respectively. It also reveals chemical bonds. Positive value indicates metallic bonds while the negative one indicates covalent bonds. In our study, the Cauchy pressure of $CaFe_2As_2$ is −3.37, indicating that our compound is brittle with covalent bonding characteristics. Brittle materials like the ceramics which have a wide range of properties hence used for multiple applications.

3.2. Electronic Structure Properties

We present the band structure and projected density of states of $CaFe_2As_2$. The band structure of $CaFe_2As_2$ shown in **Figure 2** was computed along high symmetry points; Γ-X-N-X-N-Γ.

Fermi level is at the center between the conduction band and the valence band, separating the particles in each band with specific quantum states from

Table 3. Mechanical properties of Bulk, Shear, Young's moduli and Poisson's ratioin GPa.

Voigt-Reuss Reuss Approx.	Voigt-Reuss Hill	Approximation	Average
Bulk Modulus (*B*) (GPa)	44.55	43.88	44.21
Young Modulus (*E*) (GPa)	68.39	66.40	67.40
Shear Modulus (*G*) (GPa)	27.48	26.60	67.40
Poisson's Ration (*n*)	0.24	0. 25	0.25

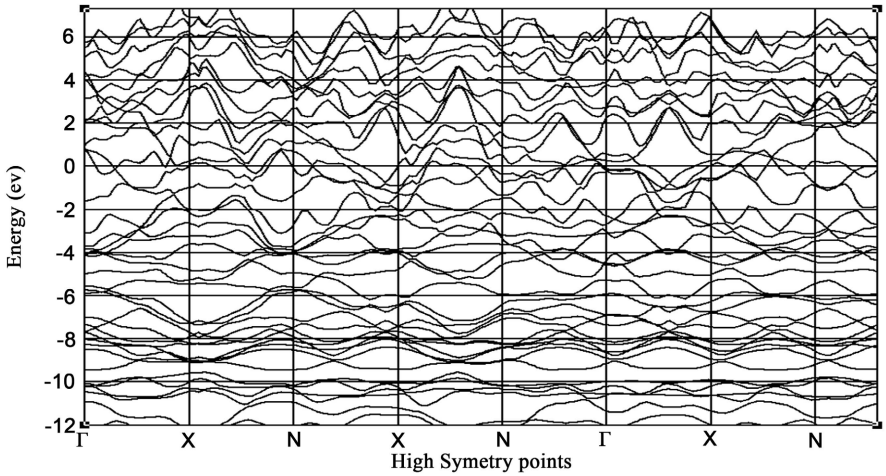

Figure 2. Band structure of $CaFe_2As_2$ showing that it is metallic in nature.

interacting [37]. From **Figure 2**, it is seen that the conduction band and valence band are overlapping, which is a clear indication that the compound is metallic and compares well with $ThCr_2As_2$ [38]. The projected density of states of $CaFe_2As_2$ is shown in **Figure 3**.

The iron pnictide materials are formed in layered structures with charge reservoirs insulating the layers which contribute a lot in enhancing superconductivity. Iron based superconductors have a formation of constructive 2-D structure with irregular charge reservoir. For instance, $CaFe_2As_2$ has a tetragonal structure at room temperature and transit to orthorhombic upon subjection to pressure.

From the angle resolved photoemission spectroscopy studies together with electronic structure calculations, it is quite evident that the neighborhood Fermi level is made up of Fe d states (**Figure 3(d)**). Fe 3d states that have a photoelectronic cross-section of around 10 times that of As p states in between the phonon energy. In **Figure 3(b)**, Ca, p also exhibits the higher binding energy between the range of −3 ev and 3 ev. $CaFe_2As_2$ splits at Ca layer keeping half of the calcium atoms on each side of the split surface which shows the reconstruction hence the electronic properties of Ca are different from that of bulk Ca.

The contributions of Ca, d states are basically above the energy region with a nominal contribution at or below the energy region. In the Fe-d and As-d, the contribution below the energy region shows a shift to the lower energies in the

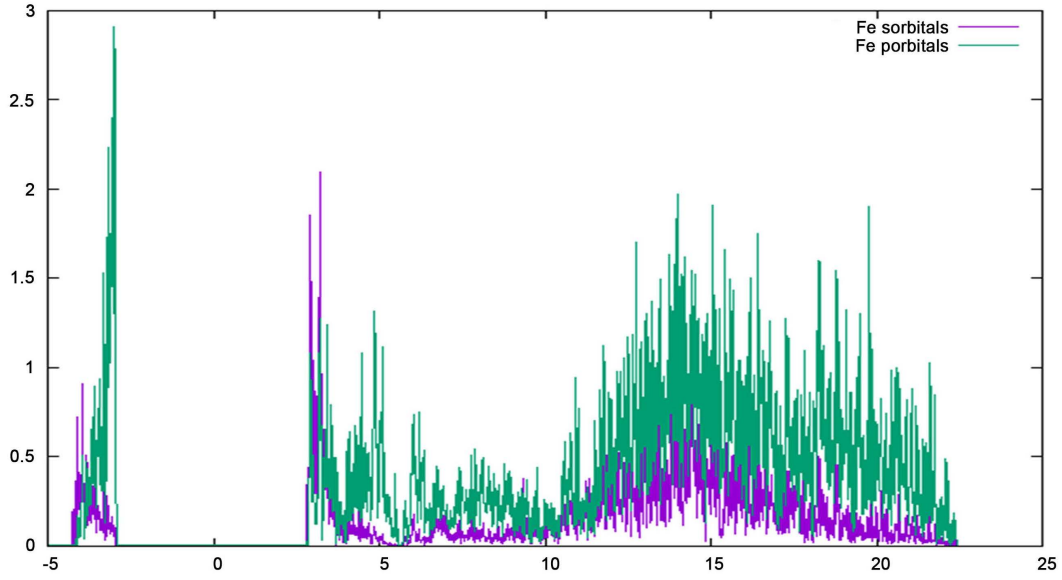
Fe sorbitals
Fe porbitals
3
2.5
2
1.5
1
0.5
0
-5
0
5
10
15
20
25

(a)

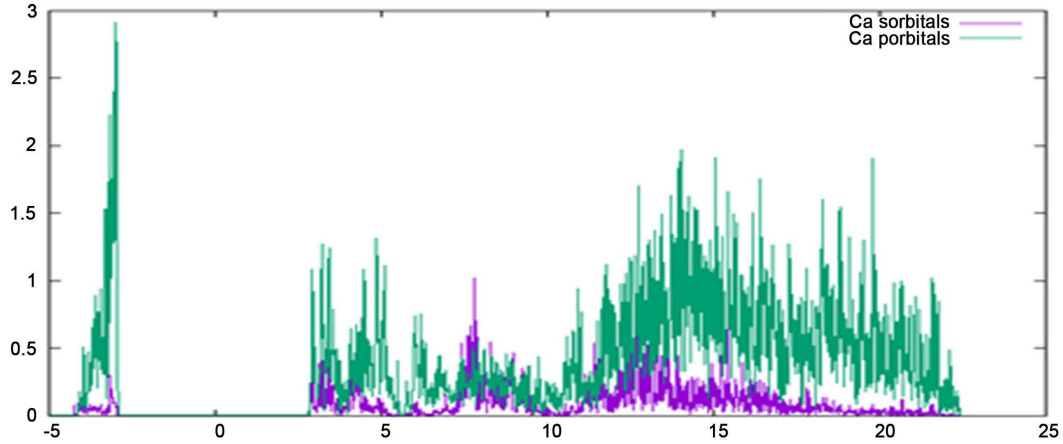
Ca sorbitals
Ca porbitals
3
2.5
2
1.5
1
0.5
0
-5
0
5
10
15
20
25

(b)

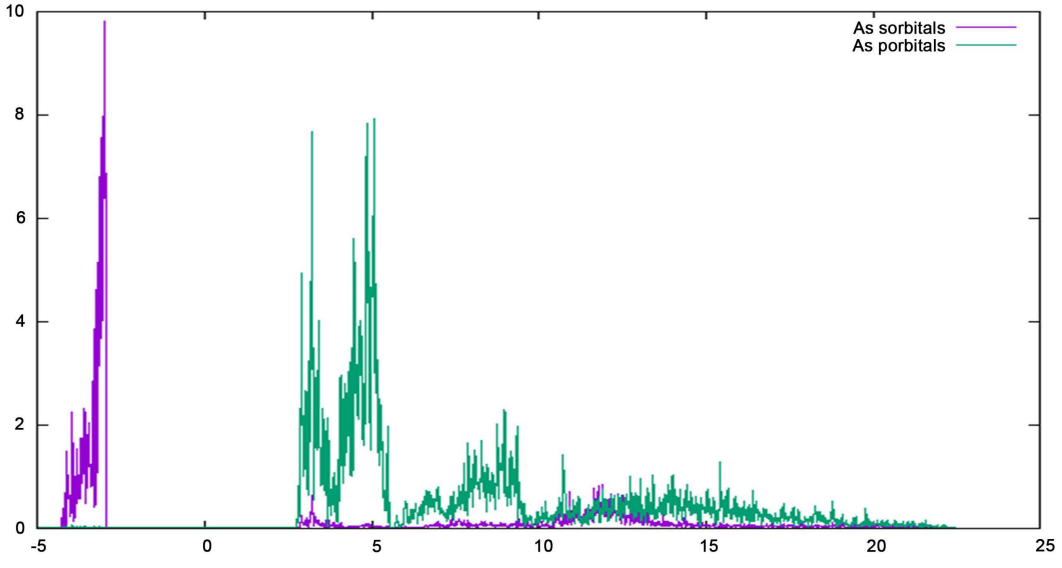
As sorbitals
As porbitals
10
8
6
4
2
0
-5
0
5
10
15
20
25

(c)

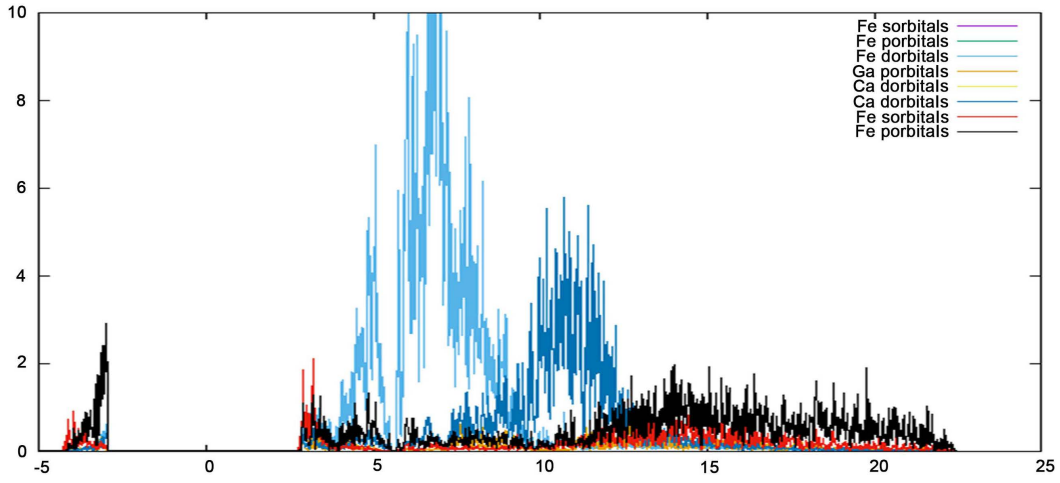

(d)

Figure 3. (a) The Projected Density of states of *Fe p*- and *s*-orbitals shows that they are more dominant in the conduction band; (b) The Projected Density of States of *Cap*- and *s*-orbitals participates majorly in the conduction band of $CaFe_2As_2$; (c) The Projected Density of States of *p*- and *s*-orbitals. *p*-states are more dominant in the conduction band than the *s*-states; (d) The total Projected Density of States of orbitals for $CaFe_2As_2$.

tetragonal phase that keeps the PDOS energy region approximately at the same energy range for both tetragonal and orthorhombic structural phases. From **Figure 1**, Ca layers are packed among two layers and any adjustment in Ca state below the energy region is as a result of the hybridization of Ca s-states with the electronic states attributed to As in the valence band [38]. The compression at the c-axis as a result of the transition to the tetragonal state brought about by the subjection to an external pressure, which brings about reduction of the separation distance between As and Ca atomic layers which results in the enhancement of Ca s and As p. Even though it is evident that the contribution of Ca in the valence band is not much, its role in the structural change and electronic structure cannot be ignored. The *S* electrons in the cations play a key role in standardizing disorder effects and pairing interactions.

3.3. Phase Transition

$CaFe_2As_2$ compound has a tetragonal phase as the stable phase with five atoms; one Ca, two Fe, and two as which upon subjection to external pressure undergoes a phase transition to the orthorhombic phase, **Figure 4** below. $CaFe_2As_2$ tetragonal stable phase undergoes a phase transition at an external pressure of 0.2 GPa to the orthorhombic phase.

Phase transition of this compound from the stable phase tetragonal to orthorhombic occurs at ground state temperature and external pressure of 0.2 GPa as shown in **Figure 5**. Phase transition occurs when the enthalpy and pressure changes are the same or nearly the same [39]. These two changes are indicated by two curves of different colors. Where the two lines coincide is the phase transition pressure and in this case is the best at 0.2 GPa.

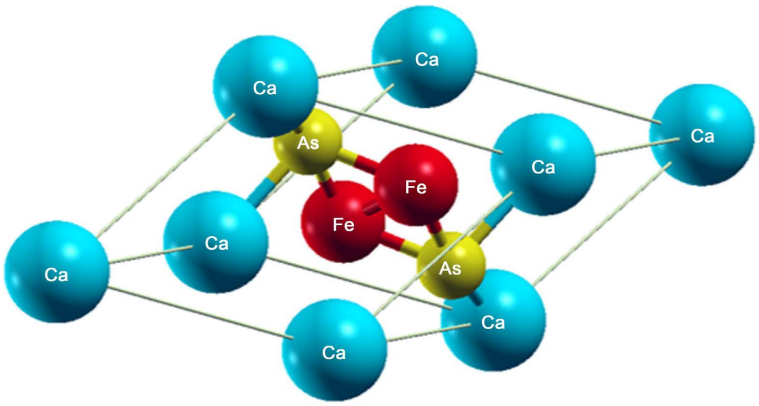

Figure 4. Orthorhombic crystal structure with cell parameters $a = b \neq c$.

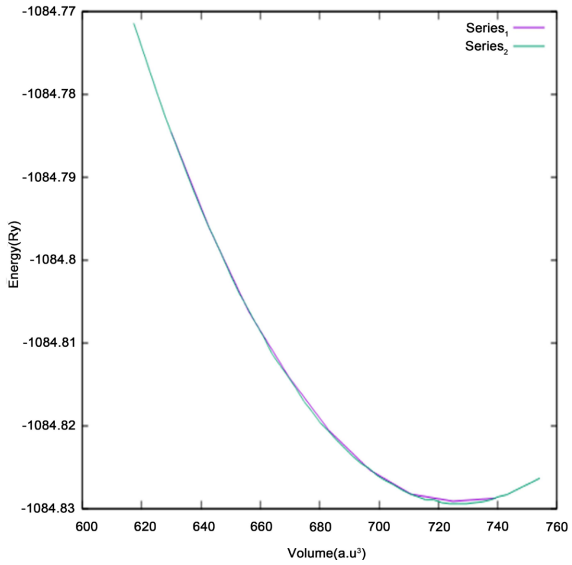

(a) Pressure = 0.1 GPa

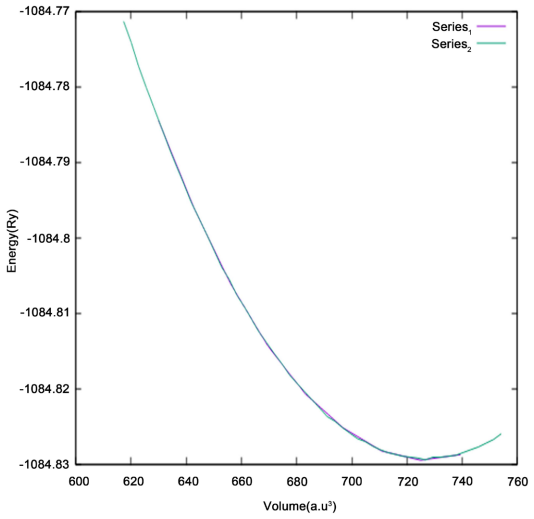

(b) Pressure = 0.2 GPa

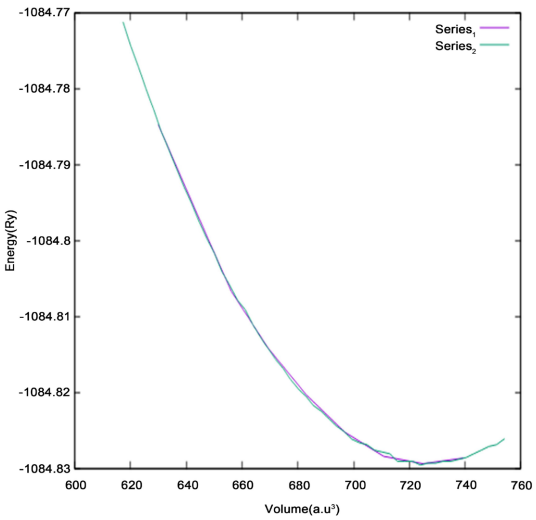

(c) Pressure = 0.3 GPa

Figure 5. Graphs of Volume against Energy for applied pressure of 0.1 GPa, 0.2 GPa, and 0.3 GPa. The best fit occurs at 0.2 GPa where the two lines properly coincide.

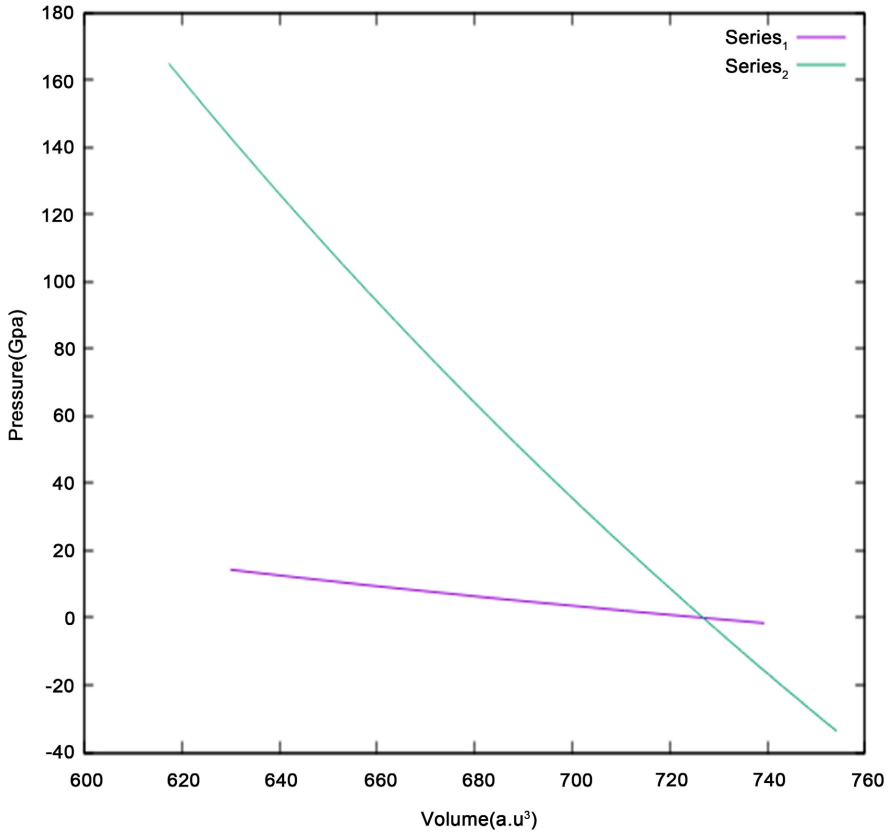

Figure 6. Graph of internal pressure against internal volume at an external pressure of 0.2 GPa.

Heat is a form of energy and the internal energy of this material changes as heat is transferred into or out of it as shown in **Figure 6**. Before the phase transition and after, the minimum energy and the enthalpy are quite different. **Figure 6** is in agreement with **Figure 5** with the phase transition at 0.2 GPa. This is in good agreement with the related studies showing that the pressure suppresses structural phase transition at low temperature stabilizing superconductivity [39]. The product of pressure and volume enables the measurement of energy within the material even when the system does not work with the surrounding. In **Figure 6**, clearly shows the estimated transition pressure which is 0.2 GPa and internal volume at about 730 $a.u^3$.

4. Conclusion

We have here reported density functional theory calculations of electronic, mechanical and pressure induced phase transition of $CaFe_2As_2$. The electronic structure calculations show that this material is metallic based on its band structure. From calculations of elastic constants, mechanical properties have been analyzed indicating that this material is brittle. Elastic constants show that $CaFe_2As_2$ is isotropic just like its parent compound $ThCr_2Si_2$. The material undergoes a structural phase change at an external pressure of 0.2 GPa from the tetragonal stable phase to orthorhombic at ground state temperature. Further stu-

dies could be made on the superconducting properties of $CaFe_2As_2$ and especially phase transition temperature T_c and magnetic transition properties.

Acknowledgements

I want to extend my gratitude to the Center for High-Performance Computing (CHPC), Cape Town, the Republic of South Africa, for the provision of HPC cluster resources that was necessary in this computational study.

Conflicts of Interest

The authors declare no conflicts of interest regarding the publication of this paper.

References

[1] Capitani, F., Langerome, B., Brubach, J.-B., Roy, P., Drozdov, A., Eremets, M., *et al.* (2017) Spectroscopic Evidence of a New Energy Scale for Superconductivity in H_3S. *Nature Physics*, **13**, 859-863. https://doi.org/10.1038/nphys4156

[2] Shrivastava, S.K. and Kumar, G. (2019) High-tc Superconductivity in Iron-Based Pnictides and Chalcogenides. *International Journal of Emerging Technologies and Innovative Research*, **6**, 417-426.

[3] Hosono, H., Tanabe, K., Takayama-Muromachi, E., Kageyama, H., Yamanaka, S., Kumakura, H., *et al.* (2015) Exploration of New Superconductors and Functional Materials, and Fabrication of Superconducting Tapes and Wires of Iron Pnictides. *Science and Technology of Advanced Materials*, **16**, Article ID: 033503. https://doi.org/10.1002/chin.201540228

[4] Soliman, S. (2016) The Stacking of Antifluorite Fe_2P_2 Layer on the Electronic Structure of the Ternary Compounds $CaFe_2P_2$, $BaFe_2P_2$ and $EuFe_2P_2$. *Computational Materials Science*, **122**, 177-182. https://doi.org/10.1016/j.commatsci.2016.05.027

[5] Cui, J. (2017) Studies of Energy-Relevant Materials by Nuclear Magnetic Resonance. Iowa State University, Ames. https://doi.org/10.2172/1417981

[6] Bud'ko, S.L., Ma, X., Tomić, M., Ran, S., Valentí, R. and Canfield, P.C. (2016) Transition to Collapsed Tetragonal Phase in $CaFe_2As_2$ Single Crystals as Seen by ^{57}Fe Mössbauer Spectroscopy. *Physical Review B*, **93**, Article ID: 024516. https://doi.org/10.1103/PhysRevB.93.024516

[7] Sanna, A., Profeta, G., Massidda, S. and Gross, E. (2014) First-Principles Study of Superconducting Rare-Earth Doped $CaFe_2As_2$. *Physical Review B*, **86**, Article ID: 014507.

[8] Polyakov, A. (2013) Fermi-Surface Investigations of Rare-Earth Transition-Metal Compounds.

[9] Dhaka, R., Jiang, R., Ran, S., Bud'ko, S.L., Canfield, P.C., Harmon, B.N., *et al.* (2014) Dramatic Changes in the Electronic Structure upon Transition to the Collapsed Tetragonal Phase in $CaFe_2As_2$. *Physical Review B*, **89**, Article ID: 020511. https://doi.org/10.1103/PhysRevB.89.020511

[10] Mishra, S., Mittal, R., Krishna, P., Sastry, P., Chaplot, S., Babu, P., *et al.* (2013) Evidence for Anomalous Structural Behavior in $CaFe_2As_2$.

[11] Sidorov, V., Lu, X., Park, T., Lee, H., Tobash, P., Baumbach, R., *et al.* (2013) Pressure Phase Diagram and Quantum Criticality of $CePt_2In_7$ Single Crystals. *Physical Review B*, **88**, Article ID: 020503. https://doi.org/10.1103/PhysRevB.88.020503

[12] Saparov, B., Cantoni, C., Pan, M., Hogan, T.C., Ii, W.R., Wilson, S.D., *et al.* (2014) Complex Structures of Different $CaFe_2As_2$ Samples. *Scientific Reports*, **4**, Article No. 4120. https://doi.org/10.1038/srep04120

[13] Shahi, P., Sun, J., Wang, S., Jiao, Y., Chen, K., Sun, S., *et al.* (2018) High-Tc Superconductivity up to 55 K under High Pressure in a Heavily Electron Doped $Li_{0.36}(NH_3)_yFe_2Se_2$ Single Crystal. *Physical Review B*, **97**, Article ID: 020508. https://doi.org/10.1103/PhysRevB.97.020508

[14] Parvin, F. and Naqib, S. (2019) Structural, Elastic, Electronic, Thermodynamic, and Optical Properties of Layered $BaPd_2As_2$ Pnictide Superconductor: A First Principles Investigation. *Journal of Alloys and Compounds*, **780**, 452-460. https://doi.org/10.1016/j.jallcom.2018.12.021

[15] Materne, P., Kamusella, S., Sarkar, R., Goltz, T., Spehling, J., Maeter, H., *et al.* (2015) Coexistence of Superconductivity and Magnetism in $Ca_{1-x}Na_xFe_2As_2$: Universal Suppression of the Magnetic Order Parameter in 122 Iron Pnictides. *Physical Review B*, **92**, Article ID: 134511. https://doi.org/10.1103/PhysRevB.92.134511

[16] Idrissi, S., Labrim, H., Bahmad, L. and Benyoussef, A. (2021) DFT and TDDFT Studies of the New Inorganic Perovskite $CsPbI_3$ for Solar Cell Applications. *Chemical Physics Letters*, **766**, Article ID: 138347. https://doi.org/10.1016/j.cplett.2021.138347

[17] Idrissi, S., Mounkachi, O., Bahmad, L. and Benyoussef, A. (2022) Study of the Electronic and Opto-Electronic Properties of the Perovskite $KPbBr_3$ by DFT and TDDFT Methods. *Computational Condensed Matter*, **33**, e00617. https://doi.org/10.1016/j.cocom.2021.e00617

[18] Felipe, H., Qiu, D.Y. and Louie, S.G. (2017) Nonuniform Sampling Schemes of the Brillouin Zone for Many-Electron Perturbation-Theory Calculations in Reduced Dimensionality. *Physical Review B*, **95**, Article ID: 035109. https://doi.org/10.1103/PhysRevB.95.035109

[19] Sypek, J.T., Yu, H., Dusoe, K.J., Drachuck, G., Patel, H., Giroux, A.M., *et al.* (2017) Superelasticity and Cryogenic Linear Shape Memory Effects of $CaFe_2As_2$. *Nature Communications*, **8**, Article No. 1083. https://doi.org/10.1038/s41467-017-01275-z

[20] Hadi, M., Roknuzzaman, M., Chroneos, A., Naqib, S., Islam, A., Vovk, R., *et al.* (2017) Elastic and Thermodynamic Properties of New $(Zr_{3-x}Ti_x)AlC_2$ MAX-Phase Solid Solutions. *Computational Materials Science*, **137**, 318-326. https://doi.org/10.1016/j.commatsci.2017.06.007

[21] Sangeetha, N., Smetana, V., Mudring, A.-V. and Johnston, D. (2018) Antiferromagnetism in Semiconducting $SrMn_2Sb_2$ and $BaMn_2Sb_2$ Single Crystals. *Physical Review B*, **97**, Article ID: 014402. https://doi.org/10.1103/PhysRevB.97.014402

[22] Biskri, Z.E., Rached, H., Bouchear, M. and Rached, D. (2014) Computational Study of Structural, Elastic and Electronic Properties of Lithium Disilicate ($Li_2Si_2O_5$) Glass-Ceramic. *Journal of the Mechanical Behavior of Biomedical Materials*, **32**, 345-350. https://doi.org/10.1016/j.jmbbm.2013.10.029

[23] Luan, X., Qin, H., Liu, F., Dai, Z., Yi, Y. and Li, Q. (2018) The Mechanical Properties and Elastic Anisotropies of Cubic Ni_3Al from First Principles Calculations. *Crystals*, **8**, Article No. 307. https://doi.org/10.3390/cryst8080307

[24] Toher, C., Plata, J.J., Levy, O., De Jong, M., Asta, M., Nardelli, M.B., *et al.* (2014) High-Throughput Computational Screening of Thermal Conductivity, Debye Temperature, and Grüneisen Parameter Using a Quasiharmonic Debye Model. *Physical Review B*, **90**, Article ID: 174107. https://doi.org/10.1103/PhysRevB.90.174107

[25] Rabah, M., Benalia, S., Rached, D., Abidri, B., Rached, H. and Vergoten, G. (2010)

Prediction of Stabilities Phase and Elastic Properties of Palladium Carbide. *Computational Materials Science*, **48**, 556-562. https://doi.org/10.1016/j.commatsci.2010.02.023

[26] Zhang, Y. and Zhang, J. (2014) First Principles Study of Structural and Thermodynamic Properties of Zirconia. *Materials Today*: *Proceedings*, **1**, 44-54. https://doi.org/10.1016/j.matpr.2014.09.011

[27] Jayasekara, W., Pandey, A., Kreyssig, A., Sangeetha, N., Sapkota, A., Kothapalli, K., *et al.* (2017) Suppression of Magnetic Order in $CaCo_{1.86}As_2$ with Fe Substitution: Magnetization, Neutron Diffraction, and X-Ray Diffraction Studies of $Ca(Co_{1-x}Fe_x)_yAs_2$. *Physical Review B*, **95**, Article ID: 064425.

[28] Wei, F., Lv, B., Deng, L., Meen, J.K., Xue, Y.-Y. and Chu, C.-W. (2014) The Unusually High Tc in Rare-Earth-Doped Single Crystalline $CaFe_2As_2$. *Philosophical Magazine*, **94**, 2562-2570. https://doi.org/10.1080/14786435.2014.913116

[29] Li, J., Yu, J., Wu, S. and Xie, J. (2022) The Mechanical Resistance of Asphalt Mixture with Steel Slag to Deformation and Skid Degradation Based on Laboratory Accelerated Heavy Loading Test. *Materials*, **15**, Article No. 911. https://doi.org/10.3390/ma15030911

[30] Kvashnina, Y.A., Kvashnin, A., Popov, M.Y., Kulnitskiy, B., Perezhogin, I., Tyukalova, E., *et al.* (2015) Toward the Ultra-Incompressible Carbon Materials. Computational Simulation and Experimental Observation. *The Journal of Physical Chemistry Letters*, **6**, 2147-2152. https://doi.org/10.1021/acs.jpclett.5b00748

[31] Zaddach, A., Niu, C., Koch, C. and Irving, D. (2013) Mechanical Properties and Stacking Fault Energies of NiFeCrCoMn High-Entropy Alloy. *Jom*, **65**, 1780-1789. https://doi.org/10.1007/s11837-013-0771-4

[32] Jayalakshmi, D., Sundareswari, M., Viswanathan, E., Hemanand, D. and Pranesh, V. (2019) Computational Study on Unconventional Superconductivity and Mechanical Properties of Novel Antiferrromagnetic (Ca, Sr, Ba) Fe_2Bi_2 Compounds. *International Journal of Modern Physics B*, **33**, Article ID: 1950341. https://doi.org/10.1142/S0217979219503417

[33] Rahman, M.A., Rahaman, M.Z. and Rahman, M.A. (2016) The Structural, Elastic, Electronic and Optical Properties of MgCu under Pressure: A First-Principles Study. *International Journal of Modern Physics B*, **30**, Article ID: 1650199. https://doi.org/10.1142/S021797921650199X

[34] Idrissi, S., Labrim, H., Bahmad, L. and Benyoussef, A. (2021) Study of the Solar Perovskite $CsMBr_3$ (M = Pb or Ge) Photovoltaic Materials: Band-Gap Engineering. *Solid State Sciences*, **118**, Article ID: 106679. https://doi.org/10.1016/j.solidstatesciences.2021.106679

[35] Islam, J. and Hossain, A.A. (2021) Investigation of Physical and Superconducting Properties of Newly Synthesized $CaPd_2P_2$ and $SrPd_2P_2$. *Journal of Alloys and Compounds*, **868**, Article ID: 159199. https://doi.org/10.1016/j.jallcom.2021.159199

[36] Ali, K. and Maiti, K. (2017) Emergent Electronic Structure of $CaFe_2As_2$. *Scientific Reports*, **7**, Article No. 6298. https://doi.org/10.1038/s41598-017-06591-4

[37] Agora, J.O., Otieno, C., Nyawere, P.W. and Manyali, G.S. (2020) *Ab Initio* Study of Pressure Induced Phase Transition, Structural and Electronic Structure Properties of Superconducting Perovskite Compound $GdBa_2Cu_3O_{7-x}$. *Computational Condensed Matter*, **23**, e00461. https://doi.org/10.1016/j.cocom.2020.e00461

[38] Chen, D.-Y., Yu, J., Ruan, B.-B., Guo, Q., Zhang, L., Mu, Q.-G., *et al.* (2016) Superconductivity in Undoped $CaFe_2As_2$ Single Crystals. *Chinese Physics Letters*, **33**, Article ID: 067402. https://doi.org/10.1088/0256-307X/33/6/067402

[39] Nyawere, P.W.O., Makau, N.W. and Amolo, G.O. (2014) First Principles Calculation of Elastic Constants of Cubic, Orthorhombic and Hexagonal Phases of BaF_2. *Physica B*, **434**, 122-128. https://doi.org/10.1016/j.physb.2013.10.051